



**UNIVERSITY OF LEEDS**

This is a repository copy of *DC voltage control for MMC-based railway power supply integrated with renewable generation*.

White Rose Research Online URL for this paper:  
<http://eprints.whiterose.ac.uk/166347/>

Version: Accepted Version

---

**Article:**

Sun, P [orcid.org/0000-0001-8061-224X](https://orcid.org/0000-0001-8061-224X), Li, K [orcid.org/0000-0001-6657-0522](https://orcid.org/0000-0001-6657-0522), Li, Y et al. (1 more author) (2020) DC voltage control for MMC-based railway power supply integrated with renewable generation. *IET Renewable Power Generation*, 14 (18). pp. 3679-3689. ISSN 1752-1424

<https://doi.org/10.1049/iet-rpg.2020.0132>

---

This item is protected by copyright. This is an author produced version of an article accepted for publication in *IET Renewable Power Generation*. Uploaded in accordance with the publisher's self-archiving policy.

**Reuse**

Items deposited in White Rose Research Online are protected by copyright, with all rights reserved unless indicated otherwise. They may be downloaded and/or printed for private study, or other acts as permitted by national copyright laws. The publisher or other rights holders may allow further reproduction and re-use of the full text version. This is indicated by the licence information on the White Rose Research Online record for the item.

**Takedown**

If you consider content in White Rose Research Online to be in breach of UK law, please notify us by emailing [eprints@whiterose.ac.uk](mailto:eprints@whiterose.ac.uk) including the URL of the record and the reason for the withdrawal request.



[eprints@whiterose.ac.uk](mailto:eprints@whiterose.ac.uk)  
<https://eprints.whiterose.ac.uk/>

# DC Voltage Control for MMC based Railway Power Supply Integrated with Renewable Generation

Peiliang SUN, Kang LI, Yongfe LI, Li ZHANG

**Abstract**—The full controllable electronic device based railway feeder station offers better power quality and more flexible configurations than conventional transformer based stations. This paper investigates a modular multilevel converter (MMC) based static frequency converter station with renewable energy access. Wind power generation is coupled into the station via dc link of the back to back converter. The dynamic single phase traction load and intermittent renewable generation bring double frequency oscillation and large deviation problems to the dc link voltage. Special design considerations and control schemes are proposed for the MMC to stabilise dc link voltage by controlling the total number of total inserted modules. The proposed control scheme resolves the voltage oscillation issue caused by single phase load and reduces the dc link voltage deviation under 10 MW step change. A series of device based simulations validate the control scheme which realises a reliable coupling interface for connecting the renewable generation to the dc bus.

**Index Terms**—railways, modular converter, back to back converters, power supply system.

## NOMENCLATURE

$\Delta u_{dc}^{ref}$  DC link voltage stabilisation control reference  
 $\Delta u_{Cju}^i, \Delta u_{Cjl}^i$  The  $i$ th capacitor voltage balance control references for upper and lower branch of MMC phase  $j$   
 MMC<sub>G</sub> Grid side converter  
 MMC<sub>L</sub> Traction line side converter  
 $\omega$  Angular velocity of the grid  
 $\omega_e^M$  Wind generator electrical angular speed  
 $\omega_r$  Resonant angular velocity of the resonant controller  
 $\psi_m$  Wind generator rotor flux linkage  
 $\varphi$  Traction load angle  
 $a$  Average capacitor voltage factor  
 $C_{sub}$  MMC submodule capacitor  
 $i_{ga}, i_{gb}, i_{gc}$  Three phase current at the grid side of MMC  
 $i_o$  Output current of the traction line side MMC  
 $i_d, i_q$  The  $d$  and  $q$  axis current of the grid side MMC  
 $i_d^M, i_q^M$   $d$  and  $q$  axis current of the wind generator  
 $i_{dc}$  MMC dc link current  
 $i_{jcom}$  Common mode current of MMC phase  $j$ ,  $j = a, b, c, e, f$   
 $i_{jdif}$  Differential mode current of MMC phase  $j$ ,  $j = a, b, c, e, f$   
 $i_{jl}$  Current in the MMC phase  $j$  lower branch,  $j = a, b, c, e, f$   
 $i_{ju}$  Current in the MMC phase  $j$  upper branch,  $j = a, b, c, e, f$   
 $L_m^M$  Wind generator synchronous inductance  
 $L_{br}$  MMC branch inductor

$m_{jcom}$  Common mode modulation index of MMC phase  $j$ ,  $j = a, b, c, e, f$   
 $m_{jdif}$  Differential mode modulation index of MMC phase  $j$ ,  $j = a, b, c, e, f$   
 $m_{jl}$  Modulation index of MMC phase  $j$  upper branch,  $j = a, b, c, e, f$   
 $m_{ju}$  Modulation index of MMC phase  $j$  upper branch,  $j = a, b, c, e, f$   
 $N$  Number of submodules in one MMC phase  
 $p_{grid}$  Instantaneous power measured at grid side  
 $P_G$  Grid side power  
 $P_L$  Traction load power  
 $p_{mmc}$  Instantaneous power measured at MMC dc link  
 $p_{pmsg}$  Instantaneous power converted by wind generator  
 $p_{train}$  Instantaneous power consumed by traction load  
 $P_W$  Wind power generation  
 $R_s^M$  Wind generator stator winding resistance  
 $R_{br}$  Equivalent resistance of one MMC branch  
 $T_{sc}$  Control system sampling rate  
 $u_C^{ave}$  Average capacitor voltage of MMC  
 $u_{dc}$  MMC dc link voltage  
 $u_e, u_f$  Traction line side MMC terminal voltage of phase  $e, f$   
 $u_{ga}, u_{gb}, u_{gc}$  Three phase voltage at the grid side of MMC  
 $u_o$  Output voltage of the traction line side MMC  
 $u_C^i$  Capacitor voltage of the  $i$ th submodule of MMC  
 $u_{jcir}^{ref}$  MMC phase  $j$  circulating current control reference,  $j = a, b, c$   
 $u_{jcom}$  Common mode voltage of MMC phase  $j$ ,  $j = a, b, c, e, f$   
 $u_{jdif}$  Differential mode voltage of MMC phase  $j$ ,  $j = a, b, c, e, f$   
 $u_{jl}$  Voltage of all inserted submodules in MMC phase  $j$  lower branches,  $j = a, b, c, e, f$   
 $u_{josc}^{ref}$  Traction side converter oscillation current suppression control reference in MMC phase  $j$ ,  $j = e, f$   
 $u_{ju}$  Voltage of all inserted submodules in MMC phase  $j$  upper branches,  $j = a, b, c, e, f$   
 $V_{dc}$  Nominal MMC dc link voltage  
 $v_d^M$  The  $d$  axis generator terminal voltage  
 $v_q^M$  The  $q$  axis generator terminal voltage

## I. INTRODUCTION

The landscape change of the energy sector for embracing significant renewable penetration has made the electrified railway an environmentally more friendly means of transportation than on-road vehicles and air transport. The ac power supply scheme is the most consolidated technology which enjoys

popularity in current high-speed railway applications, and the 25 kV single phase ac power supply scheme is widely adopted in the traction power supply system (TPSS) in many countries such as Japan, China, UK and France etc. However, most of the existing 25 kV ac supply feeder stations are realised by conventional transformers which lead to several power quality issues such as voltage unbalance, low power factor and harmonics issues. Various compensation schemes and balanced transformers have been researched and implemented in railway systems to improve the power quality [17].

So far, the power electronic technologies have become mature for high voltage and high power applications with the advancement of high power semiconductor switches. Full power electronic converter based railway traction feeder station have been researched and used [2]. These power electronic converter based substations are also named as "static frequency converter (SFC)" in the community and which are back to back conversion systems. The power quality issues brought by transformers can be solved in the full converter based substation. Moreover, the SFC station enables effective feeding of regenerative power back to the grid. The modular multilevel converter topology has been intensively researched in recent years and has shown its advantages in high voltage direct current (HVDC) transmission system and high power conversion applications [14, 9, 25, 20].

The successful applications of power electronic converter not only improve the power quality but also facilitate a more flexible power supply system for the future electrical railway system (ERS). In the past decade, some pioneering work has been carried out to verify the feasibility of integrating renewable energy source (RES) and energy storage system (ESS) into ERS. The European Union initiated the MERLIN project [4] to achieve a more sustainable and optimised energy usage in European electric mainline railway system in 2012. Japanese researchers demonstrated the potential of using photovoltaic (PV) panels on platform roofs and railway premises to introduce the solar power into the ERS in 2013 [7]. Zero emission operation has been achieved in a local 'Hiraizumi Station' with solar energy generation and lithium ion batteries [6].

To improve the energy efficiency, the East Japan Railway Company also studied economic benefit of the dc railway regenerative energy utilisation by energy storage system [5]. In [12], PV generation with hybrid ESS is connected to the cophase traction power system for coordinating regenerative braking energy and local renewable energy, and energy management strategy is optimised to achieve the lowest daily cost. Şengör et al. also presented a mixed-integer programming model to minimise the daily operational cost of a similar system [16] where the model considers the dynamics of train load, pricing scheme, stochastic nature of state of energy (SOE) and uncertain PV generation. Zhu et al. [26] used passivity-based stability criterion to assess the stability of a PV plant tied into medium voltage dc railway electrification system, and proposed a virtual impedance control scheme.

Railway power supply integrated with RESs and hybrid ESSs relies heavily on the ICT technologies to operate reliably, effectively and efficiently. Therefore researchers have consid-

ered the next generation of ERS to be a smart railway system, where information and communication technologies are used to improve the overall controllability. Eduardo et al. discussed key features in a smart railway system, including 'smart train operation', 'smart operation of railway power supply', and 'smart interaction with other power systems' [4].

Aguado et al. proposed a methodology for optimal operation planning of railway energy systems considering the uncertainties associated to RES through scenario tree approach [1]. Hovak et al. presented a hierarchical coordination scheme for substation energy flow control and the individual traction control, and used a stationary energy storage system to minimise energy consumption [15]. Through interactions with other power systems, the ERS is transformed from a passive energy consumer into a proactive system which has the capability to respond to various grid demands. Sun et al. evaluated the impact of battery based railway transportation on power grid operation [19], and demonstrated that the mobile battery storage can relieve the transmission congestion while reduce the operation costs.

Most of the research works mainly focus on RES and ESS installation capacity and power flow optimisation. The accurate system dynamics in medium voltage ac railway supply system with RES integration has not been fully investigated. Renewable energy such as wind and solar energy are intermittent and cannot be accurately predicted. Similarly, the traction load has similar characteristics due to rail condition, carrying weight, weather and other factors. Unlike the conventional transformer based station, the power electronic converter based station needs to be controlled in real time to transfer the energy among the grid, RES and the train. The intermittent renewable energy generation and rapid changing train load will impose more stringent requirements on the converter performance.

The instantaneous power consumed by single phase traction load introduces double frequency oscillation into the supply system [21]. The existence of sudden load change, intermittent renewable generation and oscillating single phase power challenge the stable operation of the hybrid railway power supply system.

In this paper, a full power modular multilevel converter solution is proposed for railway traction power supply integrated with RES. The aforementioned problems of single phase oscillation and high power change are addressed by utilising floating capacitor in the MMC. The remainder of the paper is organised as follows. Section II discusses the configurations of integrating RES with substation. Section III details the modelling and control of wind generation system. MMC modelling and control details are introduced in Section IV. Simulation results of several scenarios are evaluated in Section V and Section VI concludes the paper.

## II. RAILWAY TRACTION POWER SUPPLY INTEGRATED WITH RENEWABLE GENERATIONS

### A. Topologies

Six different configurations with RES integrated into railway traction supply system are illustrated in Fig. 1. Configurations presented in Figures 1a and 1b do not need any modification in the original stations, RES is directly connected to the

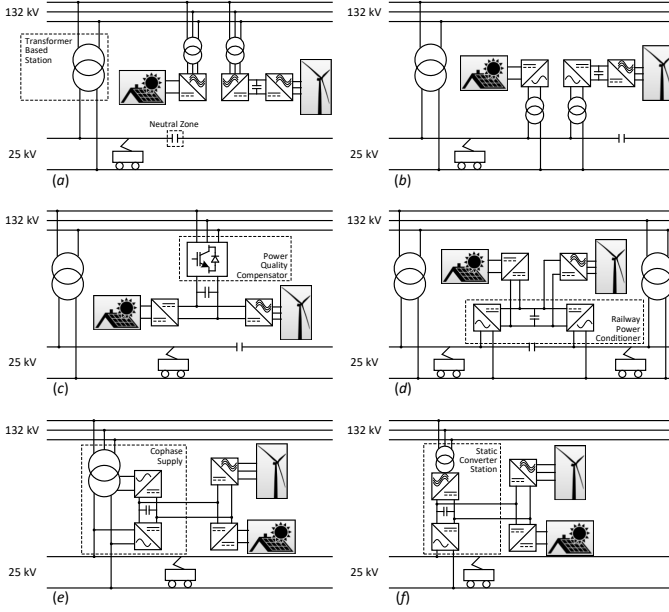


Fig. 1: Different connection schemes for integrating renewable energy source into railway supply system

- a RES interfaced with high voltage distribution grid
- b RES interfaced with medium voltage 25 kV overhead line
- c RES interfaced with power grid compensator
- d RES interfaced with railway power conditioner
- e RES interfaced with cophase supply conditioner
- f RES interfaced with static converter based station

power grid or traction overheadline. These two configurations are typical in conventional smart grid and their design and control are studied in [3].

Figures 1c and 1d represent the scenarios where the RES is connected to the grid side power quality compensator or railway power conditioner so that the dc/ac converter required in Fig. 1a,1b are cancelled. Both compensator and conditioner are responsible for addressing the power quality issues due to traction load. The power generated by RES will be used to balance grid current or compensate power flow between two supply arms. RES rating is limited by the conditioner capacity which is usually a portion of the feeder station. [13] analysed a multi-port railway power conditioner of Fig. 1d.

Configurations in Figures 1e,1f integrate the renewable generation into the station. Cophase connection with RES complicates the system design but provides more flexible control for traction supply because the number of neutral zone can be reduced or eliminated. Liu et al. investigated the energy management for this connection scheme [12].

Topologies presented in Fig. 1a–1e can be used regardless of the feeder station configuration. Due to the distinctive benefits of SFC based substation [10], configurations illustrated in Fig. 1f is investigated in this paper, where RES are connected to the medium dc voltage link of the back to back converter. Railway feeder stations usually have power rating from 10 MW to 80 MW, so this topology has the capacity to accept more renewable generations than configurations illustrated in Fig. 1c–1e.

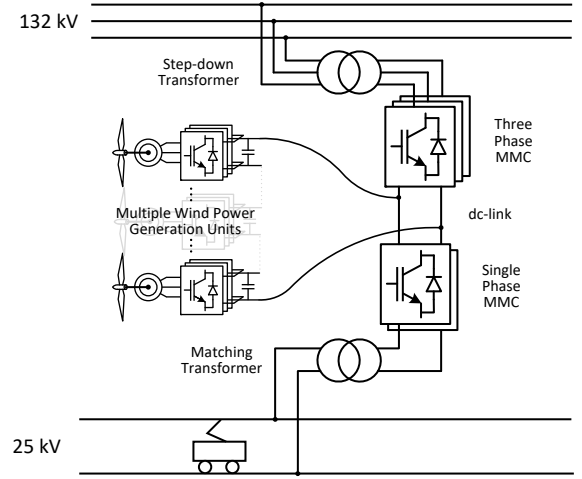


Fig. 2: Configuration of a wind power connection into static converter based railway substation

### B. The proposed static converter station integrated with wind power generation

Figure 2 presents the equivalent diagram of the proposed supply system. MMC back to back converter is used to convert three phase voltage power into single phase. As illustrated in Fig. 3, the MMC on the grid side is denoted as  $MMC_G$  and MMC connected to the traction overhead line is denoted as  $MMC_L$ . The wind turbine generator (WTG) system brings power  $P_W$  into the dc link, and the power flow of  $MMC_G$  denoted as  $P_G$  can be controlled in bi-direction depending on the dc link voltage.  $P_L$  denotes traction side power and is delivered by  $MMC_L$ .

The range of power flowing into or out of the grid ( $P_G$ ) is determined by wind power, train load and regenerative efficiency. Generally regeneration power will be less than 80% of the maximum traction power, so we can define the power rating of  $MMC_G$  as:

$$\begin{aligned} \max(P_G^+) &\geq P_L^{\max} \\ \min(P_G^-) &\leq -(0.8P_L^{\max} + P_W^{\max}), \end{aligned} \quad (1)$$

where  $P_G^+$  denotes power flowing from the grid to dc link via  $MMC_G$ ,  $P_G^-$  denotes power from dc link back to the grid via  $MMC_G$ ,  $P_L^{\max}$  and  $P_W^{\max}$  denote the maximum wind power generation and traction load power respectively. However if extra ESS is included in this system, then more wind power can be accepted without increase  $MMC_G$ 's power rating. Different power flow patterns and the symbol definition are illustrated in Fig. 3. Based on energy conservation principle, the following equation (ignoring the energy inside inductors) can be derived:

$$\int_{t_1}^{t_2} (P_W + P_G - P_L) dt = \sum \frac{C_{\text{sub}} [u_C^i(t_2) - u_C^i(t_1)]}{2}, \quad (2)$$

where  $C_{\text{sub}}$  represents each capacitor's capacitance in the system and  $u_C^i(t)$  is the corresponding voltage at time  $t$ . The fast and stable operation of wind power delivery and traction power supply depends on a stable dc link voltage. If the dc link

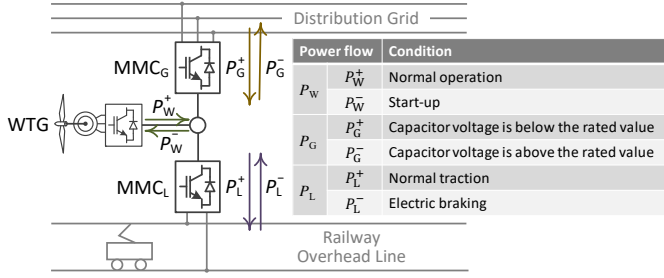


Fig. 3: Power flow illustration for the hybrid railway supply system

voltage has large deviations or large magnitude oscillations, the system performance will be compromised and the device connected to the dc-bus may behave unexpectedly [22].

As mentioned in Section I,  $P_L$  and  $P_W$  by nature have adverse effects on dc voltage stabilisation. Thus the  $MMC_G$  must robustly control dc link voltage by changing  $P_G$  and internal submodule states. Ideally, all capacitor voltages vary around their nominal values, but it is hard to achieve during transient states. For example, if  $P_L$  changes from 0 to maximum in short time in acceleration mode (or reversely in braking mode), the capacitor voltage will inevitably varies. It takes time to restore  $u_C^{ave}$  back to nominal its value and during that time dc link voltage will be affected. Section IV addresses this problem in details.

It is preferable to build wind energy conversion system (WECS) near the location of SFC station to reduce transmission losses. We assume the WECS are a set of WTGs and transmit the power through HVDC line into SFC station. There are numerous research on different topologies and control schemes for connecting wind farm and dc transmission [24]. The detailed wind farm control is beyond the scope of this paper, and therefore only one equivalent generator unit is considered for simplicity.

### III. WIND POWER GENERATOR MODELLING AND CONTROL

The wind generation system is simplified into a single machine unit. In this section, a single 10 MW permanent magnet synchronous generator (PMSG) with three phase three level neutral point clamped (NPC) converter is used to represent the WTG system Fig. 4. The medium voltage dc side of NPC connects directly to the dc link inside the SFC station

#### A. Wind power synchronous generator modelling

Figure 4 illustrates the circuit diagram of a typical wind energy conversion unit using a NPC converter. Table I lists the parameters of the equivalent WECS. Ignoring the effects of slotting, saturation, and end effect, etc., the simplified PMSG dynamic equations in  $dq$ -frame can be written as (3):

$$\begin{cases} v_d^M = R_s^M i_d^M - \omega_e^M L_q^M i_q^M + L_d^M \frac{di_d^M}{dt} \\ v_q^M = R_s^M i_q^M + \omega_e^M L_d^M i_d^M + L_q^M \frac{di_q^M}{dt} + \omega_e^M \psi_m \end{cases}, \quad (3)$$

where  $v_d^M, v_q^M$  are the machine terminal voltages in  $dq$  frame;  $\omega_e^M$  is the electrical angular speed. Here it is assumed that

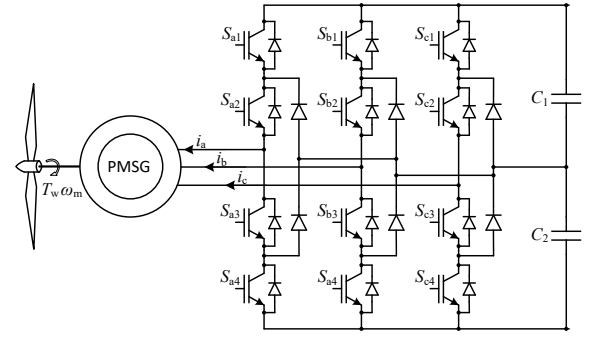


Fig. 4: Permanent magnet synchronous generator with neutral point clamped three level converter

TABLE I: System parameters of wind power generation system

PMSG machine		
Rated line voltage	$V_s^M$	26.4 kV
Rated stator frequency	$f_s^M$	20 Hz
Number of pole pairs	$p$	8
Rated rotor flux linkage	$\psi_m$	21.5 Wb
Stator winding resistance	$R_s^M$	1.6 $\Omega$
Synchronous inductance	$L_m^M$	65.6 mH
NPC converter		
Rated dc voltage	$V_{dc}$	48 kV
NPC capacitors	$C_{1,2}^M$	500 $\mu$ F
Switching frequency	$f_{npc}$	2000 Hz

<sup>1</sup> Parameters do not necessarily represent a real system

the generator is a surface mount magnet generator, viz.  $L_d^M = L_q^M = L_m^M$ . The machine parameters are shown in Table I.

The wind turbine model is also reduced to a controlled torque source. In this simplified system, the generator is controlled in constant speed operation with fast response to external torque input. We simulate different wind power generation by changing the value of applied torque on PMSG's shaft.

#### B. Generator controller design

To achieve fast response, a modified deadbeat control is adopted as machine controller. Deadbeat control is a model based control method which is equivalent to a simplified implementation of the horizon one model predictive controller. Discretize (3) using forward Euler method with controller sample time  $T_{sc}$ , the prediction of  $dq$  axis currents can be explicitly predicted:

$$\begin{bmatrix} i_d^M(k+1) \\ i_q^M(k+1) \end{bmatrix} = \begin{bmatrix} 1 - T_{sc} \frac{R_s^M}{L_m^M} & T_{sc} \omega_e^M(k) \\ -T_{sc} \omega_e^M(k) & 1 - T_{sc} \frac{R_s^M}{L_m^M} \end{bmatrix} \begin{bmatrix} i_d^M(k) \\ i_q^M(k) \end{bmatrix} + \begin{bmatrix} T_{sc} \frac{1}{L_m^M} & 0 \\ 0 & T_{sc} \frac{1}{L_m^M} \end{bmatrix} \begin{bmatrix} v_d^M(k) \\ v_q^M(k) \end{bmatrix} + \begin{bmatrix} 0 \\ -T_{sc} \frac{\omega_e^M(k) \psi_m}{L_m^M} \end{bmatrix}. \quad (4)$$

As described in Fig. 5, reference current  $i_q^{Mref}$  is updated by PI controller and  $i_d^{Mref}$  is set to zero for maximum torque per ampere control. Therefore we can calculate the required terminal voltage to generate the exact reference current in the next time step using (5).

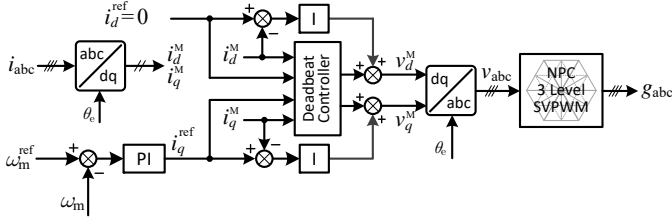


Fig. 5: Controller diagram for PMSG drive

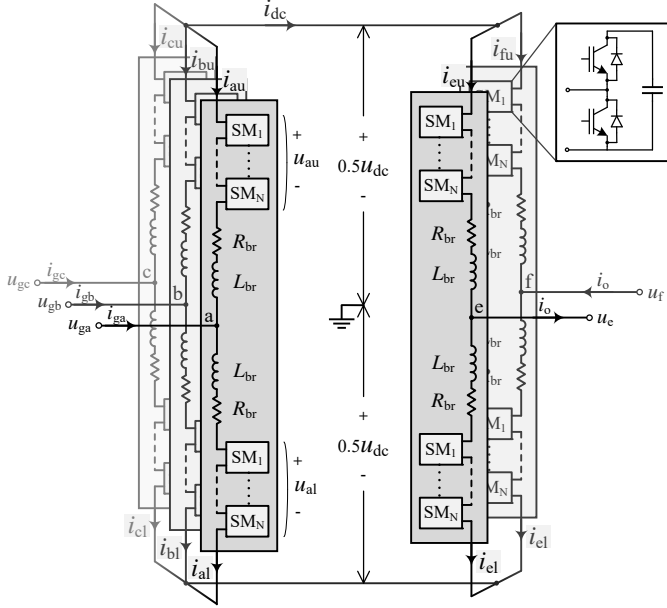


Fig. 6: Topology of the MMC back to back static converter

$$\begin{bmatrix} v_d^{Mref} \\ v_q^{Mref} \end{bmatrix} = \begin{bmatrix} R_s^M - \frac{1}{T_{sc}} L_m^M & -L_m^M \omega_e^M(k) \\ L_m^M \omega_e^M(k) & R_s^M - \frac{1}{T_{sc}} L_m^M \end{bmatrix} \begin{bmatrix} i_d^M(k) \\ i_q^M(k) \end{bmatrix} + \begin{bmatrix} \frac{1}{T_{sc}} L_m^M & 0 \\ 0 & \frac{1}{T_{sc}} L_m^M \end{bmatrix} \begin{bmatrix} i_d^{Mref} \\ i_q^{Mref} \end{bmatrix} + \begin{bmatrix} 0 \\ \psi_m \omega_e^M(k) \end{bmatrix} \quad (5)$$

Equation (5) expresses the control equations inside the dead-beat controller which calculate terminal voltage command to control  $i_d^M, i_q^M$  to track the reference signal without error. However the sampling time  $T_{sc}$  cannot be infinitesimal, so modelling error deteriorates its current control performance. For this reason, parallel integral controllers are added (Fig. 5) to improve the control robustness [11]. The composite voltage command signals are then transformed back to abc frame and the space vector pulse width modulation method (SVPWM) is used to decide switching states in the NPC controller.

#### IV. MMC BASED STATIC FREQUENCY CONVERTER STATION

##### A. Modelling and design of the back to back converter

###### 1) Single phase model and control principle of MMC:

Figure 6 shows the circuit topology of MMC-based static back to back converter. The back to back converter has three phases (a, b, c) working as a grid connection converter and two phases (e, f) connecting with railway traction overhead line. Different

phases have similar structure and each of them is composed of two sets of series connected half-bridge modules with branch inductor  $L_{br}$ . The dc link voltage is measured as  $u_{dc}$ , and a virtual reference point is used to derive circuit equations.  $u_{ga}, u_{gb}, u_{gc}$  are three phase voltages with star connection, and thus  $i_{ga} + i_{gb} + i_{gc} = 0$ . For simplicity, we consider discuss the single phase MMC model in the following explanation.

Symbols  $u_{ju}$  and  $u_{jl}$  represent the voltage of all inserted modules in upper and lower branches in phase  $j$  respectively. By Kirchhoff's law the current and voltage in phase  $a$  follow (6) to (8).

$$u_{gj} = -R_{br} i_{ju} - L_{br} \frac{di_{ju}}{dt} - u_{ju} + 0.5u_{dc} \quad (6)$$

$$u_{gj} = +R_{br} i_{jl} + L_{br} \frac{di_{jl}}{dt} + u_{jl} - 0.5u_{dc} \quad (7)$$

$$i_{gj} = -i_{ju} + i_{jl} \quad (8)$$

Then add and subtract (6) and (7) the following expressions of terminal voltage  $u_{gj}$  and dc link voltage  $u_{dc}$  are obtained.

$$u_{dc} = u_{ju} + u_{jl} + 2R_{br} \frac{i_{ju} + i_{jl}}{2} + 2L_{br} \frac{d}{dt} \frac{i_{ju} + i_{jl}}{2} \quad (9)$$

$$u_{gj} = \frac{-u_{ju} + u_{jl}}{2} + R_{br} \frac{-i_{ju} + i_{jl}}{2} + L_{br} \frac{d}{dt} \frac{-i_{ju} + i_{jl}}{2} \quad (10)$$

We control MMC dynamics by switching on and off of each submodule to decide voltage of  $u_{ju}$  and  $u_{jl}$ . If the number of submodules  $N \rightarrow \infty$  or the switching frequency is sufficiently high, we can use modulation indices  $m_{ju}, m_{jl}$  to represent the branch voltages:

$$u_{ju} = m_{ju} N u_C^{ave}, \quad u_{jl} = m_{jl} N u_C^{ave}, \quad (11)$$

where  $u_C^{ave}$  is the average capacitor voltage.

Equation (8)–(10) imply that the ac terminal side value is decided by the difference value of upper and lower branch, and the dc side is determined by common values of two branches. Therefore it is easier to view MMC topology in differential and common mode model, and the differential/common mode values are defined in (12):

$$x_{jcom} = (x_{ju} + x_{jl})/2, \quad x_{jdif} = (-x_{ju} + x_{jl})/2, \quad (12)$$

where  $x$  represents modulation index, branch voltage or branch current, and the subscripts com, dif represent the common mode value and differential mode value respectively. For example,  $i_{jdif}$  represents the differential mode current of phase  $j$  which is defined by upper and lower branch currents  $i_{ju}$  and  $i_{jl}$ .

Then the terminal voltage and current of one MMC phase can be rewritten using differential and common mode values:

$$u_{dc} = m_{jcom} 2N u_C^{ave} + i_{jcom} 2R_{br} + \frac{d}{dt} (i_{jcom} 2L_{br}), \quad (13)$$

$$u_{gj} = m_{jdif} N u_C^{ave} + i_{jdif} R_{br} + \frac{d}{dt} (i_{adif} L_{br}), \quad (14)$$

$$i_{gj} = 2i_{jdif}. \quad (15)$$

The MMC single phase equivalent model in (13) and (14) are illustrated in Fig. 7. In brief,  $u_{gj}$  is controlled by  $m_{jdif}$  and  $u_{dc}$  is controlled by  $m_{jcom}$ . In normal steady state operation,

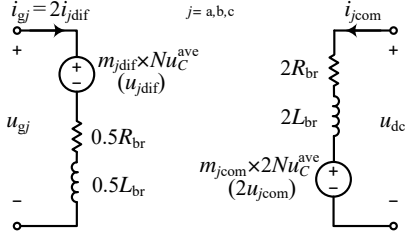


Fig. 7: Simplified equivalent differential common mode model of single MMC phase

average capacitor voltage in each branch equals to  $1/N$  of the nominal dc link voltage  $V_{dc}$ . Consequently, in most of applications,  $N$  modules are inserted in series to maintain dc link voltage at each instance by default, which gives  $m_{jcom} = 0.5$ . Usually  $i_{jcom}$  has to be controlled to suppress excessive ac components, then a small sinusoidal signal will be added to  $m_{jcom}$  to achieve this objective.

Because the differential mode shows that the MMC can be controlled in the same way as conventional two level converter, most of the previous works only stabilise dc voltage by controlling average capacitor voltages and use  $m_{jcom} = 0.5$  to indirectly maintain the dc voltage. However, if the load change drastically, namely  $i_{dc}$  change greatly in very short period of time, average capacitor voltage will no longer be the nominal value ( $u_C^{ave} \neq V_{dc}/N$ ). Modulation signal of  $m_{jcom} = 0.5$  can not guarantee stable dc link voltage and  $u_{dc}$  changes with average capacitor voltage synchronously.

The conventional approach does not fully take advantage of the special characteristics in MMC. In fact the total number of inserted submodules can be modified to compensate transient voltage drop. For this reason, it is necessary to deliberately control  $m_{jcom}$  such that dc link voltage has less deviation from the nominal value in transient state.

## 2) Parameter design of MMC back to back converter:

Assume right after a sudden load change, the average capacitor voltage becomes:

$$u_C^{ave} = a \frac{V_{dc}}{N}, \quad (16)$$

where  $a$  is the average capacitor voltage factor, and we assume  $a \in [0.5, 1.5]$ . By (13), ignoring the voltage across the inductor,  $m_{com}$  has to be set to  $0.5/a$  in order to stabilise the dc voltage perfectly.

Note that  $m_{ju}, m_{jal} \in [0, 1]$ , and therefore  $m_{adif}$  can vary from  $-0.5$  to  $0.5$  if and only if  $m_{jcom} = 0.5$ . Also in this case, the no load voltage output range is  $u_{gj} \in [-0.5V_{dc}, +0.5V_{dc}]$ . But under the condition when the average capacitor voltage has large deviation from the nominal, differential modulation range and terminal voltage are compromised if we adjust  $m_{jcom} = 0.5/a$  to maintain dc link voltage. Then the achievable ranges of modulation index and output voltage with this approach can

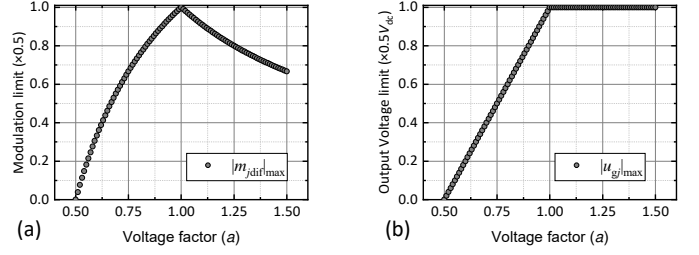


Fig. 8: Range of modulation index and output voltage with average capacitor voltage  $u_C^{ave} = aV_{dc}/N$

be expressed as follows and plotted in Fig. 8.

$$\begin{aligned} m_{jcom} &= 0.5/a \\ |m_{jdif}|_{\max} &= \begin{cases} 1 - 0.5/a, & a < 1 \\ 1/(2a), & a \geq 1 \end{cases} \quad (j = a, b, c) \quad (17) \\ |u_{gj}|_{\max} &= \begin{cases} (a - 0.5)V_{dc}, & a < 1 \\ 0.5V_{dc}, & a \geq 1 \end{cases} \end{aligned}$$

The ac terminal voltage output capability will not be affected when  $a > 1$  but decrease linearly when  $a < 1$ . Apparently, system parameters have to be carefully designed to guarantee stable operation.

Converter MMC<sub>g</sub> has to deliver power in bidirection. In no load condition, when current is small enough, the differential modulation index (denoted by  $m_{jdif1}$ ) is:

$$m_{jdif1} = \sqrt{2} \frac{V_{gn}}{V_{dc}}, \quad j = a, b, c \quad (18)$$

where  $V_{gn}$  is the phase to ground root mean square (RMS) voltage of the grid side transformer. In the rectifying mode, the differential modulation index for maximum load (denoted by  $m_{jdif2}$ ) is calculated by following equations:

$$m_{jdif2} = \frac{\sqrt{2}}{aV_{dc}} \sqrt{V_{gn}^2 + \left( \frac{PL_{eq}\pi f_g}{V_{gn}} \right)^2}, \quad P = \frac{\max(P_G^+)}{3}, \quad (19)$$

where  $f_g$  is the grid frequency,  $L_{eq}$  is the equivalent inductance which is equal to the sum of  $\frac{1}{2}L_{br}$  and the transformer leakage inductance. Similarly, in the energy feedback mode, the  $m_{jdif3}$  for maximum load is shown in (20):

$$m_{jdif3} = \frac{\sqrt{2}}{aV_{dc}} \sqrt{V_{gn}^2 + \left( \frac{PL_{eq}\pi f_g}{V_{gn}} \right)^2}, \quad P = \frac{|\min(P_G^-)|}{3}. \quad (20)$$

It is easy to see that  $m_{jdif1} < m_{jdif2} < m_{jdif3}$ , ( $j = a, b, c$ ). In normal steady state operation, the upper limit for differential modulation is 0.5 and in case of voltage deviation, the upper limit constraint is expressed in (17).  $L_{eq}$  and  $V_{gn}$  have to be designed without violating these constraints.

According to [23], the series resonance angle frequency  $\omega_{res}$  should be smaller than  $1.55\omega$  to avoid circulating current resonance. In this paper, consider the largest series resonance angular frequency of one phase:

$$\omega_{res} = \frac{1}{2} \sqrt{\frac{N/a}{2L_{br}C_{sub}}}, \quad a < 1; \quad (21)$$

TABLE II: Parameters of SFC substation back to back converter

MMC		
Transformer voltage (ph-ph)	$V_g$	21.5 kV
Rated power	$P_n$	26 MW
Rated dc voltage	$V_{dc}$	48 kV
Numbers of submodule per branch	$N$	24
Submodule capacitance	$C_{sub}$	2 mF
Branch resistance	$R_{br}$	0.5 $\Omega$
Branch inductor	$L_{br}$	18.5 mH
Switching frequency	$f_{mmc}$	500 Hz

obviously  $\omega_{res}$  has larger value when capacitor voltage is below nominal value due to a greater number of capacitors being switched on. We can design the appropriate MMC branch inductance to satisfy this criteria.

In addition to satisfying power delivery and suppressing circulating current oscillation, the MMC branch inductor also has to suppress fault current rise rate during dc link fault. To limit the magnitude of short-circuit current, the inductance value is set to 0.1 p.u. according to [18]. Consequently, the inductance in each MMC phase and transformer terminal voltage can be designed.

Assume the system changes its power supply linearly and reaches steady state after one cycle time (20 ms). Then the total energy stored in all submodules' capacitor ( $E_C^\Sigma$ ) should satisfy (22):

$$E_C^\Sigma = \frac{3}{N} C_{sub} V_{dc}^2 \geq \frac{1}{2} \frac{P_G^{\max}}{f_g \times |1 - a^2|}. \quad (22)$$

Equation (23) estimates steady state voltage ripple of the submodule capacitor in each phase. Suppose the capacitor voltage can deviate 20% of the nominal value in the worst transient load change, viz.  $0.8 \leq a \leq 1.2$ . The capacitance of each submodule  $C_{sub}$  can be designed using constraints in (22) and (23):

$$\left| \frac{\Delta u_C}{V_{dc}/N} \right|_{\max} \approx \frac{NP_j^*}{4\pi f_g C_{sub} V_{dc}^2} \frac{(1 - m_{jdif}^2)^{\frac{3}{2}}}{m_{jdif}} \leq |1 - a|_{\max}, \quad (23)$$

where  $P_j^*$  is the power rating in phase  $j$ . Table II presents the MMC parameters.

### B. AC voltage control of MMC

This section presents the control scheme to realise the ac connection to three phase power grid and single phase railway catenary. The back to back MMC generates synchronised voltage with the distribution grid and a 50 Hz sinusoidal voltage for railway power supply.

1) *Grid side converter*: The equations of three phase ac side MMC dynamics are derived in (14) and can be rewritten as:

$$\begin{cases} u_{adif} = u_{ga} - \frac{R_{br}}{2} i_{ga} - \frac{L_{br}}{2} \frac{d}{dt} i_{ga} \\ u_{bdif} = u_{gb} - \frac{R_{br}}{2} i_{gb} - \frac{L_{br}}{2} \frac{d}{dt} i_{gb} \\ u_{cdif} = u_{gc} - \frac{R_{br}}{2} i_{gc} - \frac{L_{br}}{2} \frac{d}{dt} i_{gc} \end{cases} \quad (24)$$

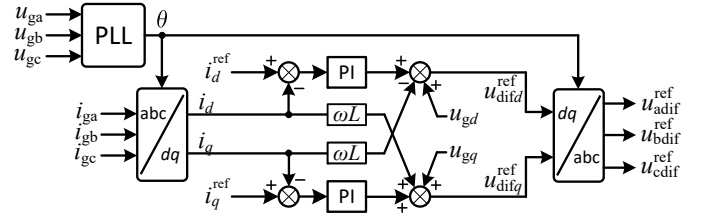


Fig. 9: Control diagram of three phase grid ac voltage controller

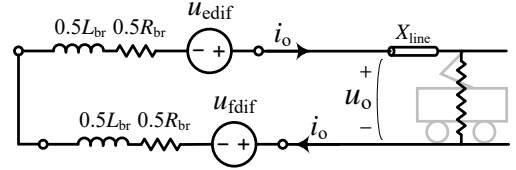


Fig. 10: Single phase MMC railway traction network supply

Use park transformation to map (24) into  $dq$  frame:

$$\begin{cases} u_{difd} = u_{gd} - \frac{R_{br}}{2} i_d - \frac{L_{br}}{2} \frac{d}{dt} i_d + \omega \frac{L_{br}}{2} i_q \\ u_{difq} = u_{gq} - \frac{R_{br}}{2} i_q - \frac{L_{br}}{2} \frac{d}{dt} i_q - \omega \frac{L_{br}}{2} i_d \end{cases}, \quad (25)$$

where  $\omega$  is the angular velocity of the grid. Equation (25) has similar form with two level converter system. The classic control method is used for outer loop control shown in Fig. 9. Three phase ac current are transformed into dc values  $i_d, i_q$  and then PI controllers with feedforward terms compose the reference values for  $u_{dif}^{\text{ref}}$  via inverse park transformation.

2) *Traction side converter*: Traction side catenary ac supply requires single phase voltage. The MMC traction side output voltage  $u_o$  is a sinusoidal voltage, and we can derive the circuit equation from the model shown in Fig. 10:

$$u_o = - \left( R_{br} i_o + L_{br} \frac{d}{dt} i_o \right) + (u_{edif} - u_{fdif}). \quad (26)$$

To maximise the difference between  $u_{edif}$  and  $u_{fdif}$ , they should be opposite to each other for maximum utilisation. Then the desired terminal voltage can be calculated as (27):

$$\begin{aligned} u_{edif} &= -u_{fdif} = \frac{1}{2} \left( u_o + R_{br} i_o + L_{br} \frac{d}{dt} i_o \right) \\ &= \left( k_p^{u_o} + \frac{k_r^{u_o} s}{s^2 + \omega^2} \right) (u_o^* - u_o) + \frac{1}{2} \left( R_{br} i_o + L_{br} \frac{d i_o}{dt} \right). \end{aligned} \quad (27)$$

The control diagram of single phase voltage supply is illustrated in Fig. 11. Because the ac voltage is directly controlled without being transformed into rotating coordinate system, proportional resonant (PR) controller is used to follow the sinusoidal reference.

### C. DC link voltage control of MMC

In ideal conditions, the dc link voltage is maintained to have as less deviation as possible. However load disturbance can cause voltage sag or swell in short time and the single phase traction load introduces doubled frequency component

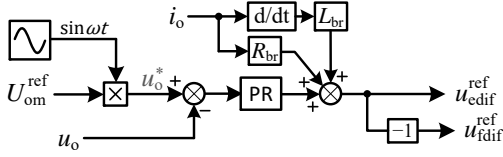


Fig. 11: Control diagram of the single phase ac traction supply

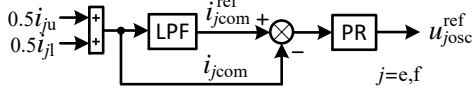


Fig. 12: DC voltage double frequency oscillation suppression

in the dc voltage. Special control based on MMC is introduced in this section.

1) *Single phase power flow oscillation suppression:* Denote MMC output voltage on railway overhead line as  $u_o$ , and load current as  $i_o$  as shown in Fig. 10. The instantaneous power consumed by traction load is  $P_L(t)$ :

$$\begin{aligned} P_L(t) &= U_{om} \sin \omega t \times I_{om} \sin(\omega t - \varphi) \\ &= \frac{U_{om} I_{om}}{2} [\cos \varphi - \cos(2\omega t - \varphi)]. \end{aligned} \quad (28)$$

In Equ.(28),  $U_{om}, I_{om}$  are the magnitude of MMC output voltage and output current respectively and  $\varphi$  is the traction load angle. Clearly, the traction load power has a double frequency component which has the comparable magnitude with its dc component. In traditional two level or multilevel NPC converters, where a shared capacitor exists, the dc link voltage will inevitably has a 100 Hz oscillating component. For example in the on-board line converter of high speed train, dc voltage rectified from single phase converter contains the 100 Hz component and affects the traction line side current [8].

In contrast, the MMC has floating capacitors and does not exchange energy from a shared capacitor. It is therefore possible to eliminate double frequency component on the dc link voltage. Referring to Fig. 6 and Fig. 7, we can have  $i_{dc} = 2i_{ecom} = 2i_{fcom}$  in steady state. Therefore rejecting ac component in  $i_{dc}$  is equal to controlling  $i_{ecom}, i_{fcom}$  to become dc values. Figure 12 shows the control diagram of this approach.

Here, calculation of the reference value common mode current  $i_{jcom}^{ref}$  is based on real time current measurement through a mean filter and thus 100 Hz signal is filtered out in calculating  $i_{jcom}^{ref}$ . Then 100 Hz component in  $i_{jcom}$  can be extracted and PR controller generates a 100 Hz control signal  $u_{josc}^{ref}$  to suppresses the oscillation current formulated in (29).

$$u_{josc}^{ref} = \left( k_p^{u_{osc}} + \frac{k_r^{u_{osc}} s}{s^2 + \omega_r^2} \right) (i_{jcom}^{ref} - i_{jcom}), \quad (29)$$

where  $\omega_r$  is the resonant frequency. With this approach, phases  $e, f$  of MMC at traction side will not introduce the oscillating power effect into the dc link at steady state. The PR controller gains are tuned by optimising the  $i_{jcom}$  tracking performance in response to the 10 MW traction load step change, where the accumulated absolute tracking error is minimised. The minimisation problem is solved by sequential quadratic programming method.

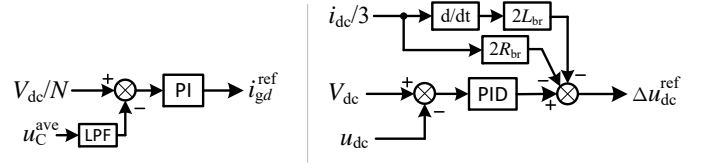


Fig. 13: DC voltage stabilisation control

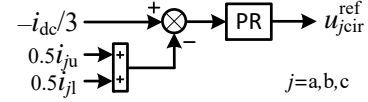


Fig. 14: Circulating current control diagram

2) *DC voltage stabilisation:* In this back to back system, the submodule capacitor voltage is maintained and stabilised by grid side converter MMC<sub>G</sub>. The capacitor voltage deviation determines the reference value of  $i_{gd}^{ref}$  by a PI controller:

$$i_{gd}^{ref} = \left( k_p^{u_c} + \frac{k_i^{u_c}}{s} \right) \left( \frac{V_{dc}}{N} - u_c^{ave} \right). \quad (30)$$

Whenever there is a sudden load change, the capacitor voltage will deviate from the nominal value, because the PI controller in (30) cannot have infinity gain and the actual system needs time to respond. According to (17), we can alter  $m_{com}$  by  $\Delta u_{dc}^{ref}$  to control the number of the inserted submodules to reduce the dc voltage deviation, as shown in (31):

$$\begin{aligned} \Delta u_{dc}^{ref} &= \left( k_p^{u_{dc}} + \frac{k_i^{u_{dc}}}{s} + k_d^{u_{dc}} \frac{N_d}{1 + N_d/s} \right) (V_{dc} - u_{dc}) \\ &\quad - 2 \left( R_{br} \frac{i_{dc}}{3} + L_{br} \frac{d i_{dc}}{dt} \frac{1}{3} \right), \end{aligned} \quad (31)$$

where  $N_d = 1000$  is the filter coefficient to realise the derivative control. Figure 13 shows the control diagram of dc voltage stabilisation control. Note that reference signals for all three phases a, b, c are controlled by the same reference  $\Delta u_{dc}^{ref}$  to avoid unnecessary circulating current between phases.

#### D. Inner control of MMC

Inner control of MMC involves circulating current control in each phase and capacitor voltage balancing in each branch.

1) *Circulating current suppression:* According to Fig. 6,  $i_{acom} + i_{bcom} + i_{ccom} = -i_{dc}$ . Also in balanced and steady state  $i_{dc}$  does not contain alternating component,  $-i_{dc}/3$  is used as common mode current reference for circulating current control. The circulating current control diagram is shown in Fig. 14 and the control reference  $u_{jcir}^{ref}$  is generated for phase  $j$  of the grid side converter.

2) *Capacitor voltage balancing:* Figure 15 illustrates the control scheme of capacitor voltage balancing in each branch where individual submodule capacitor voltage is compared with the average value. The voltage deviation will be compensated by adjusting each switching duration according to common current direction by control reference  $\Delta u_{C_{ju}}^{ref}$  and  $\Delta u_{C_{jl}}^{ref}$  for the  $i$ th submodule in phase  $j$ .

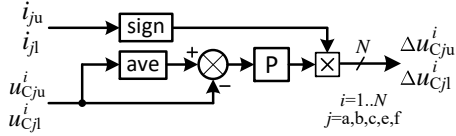


Fig. 15: Capacitor balance control diagram

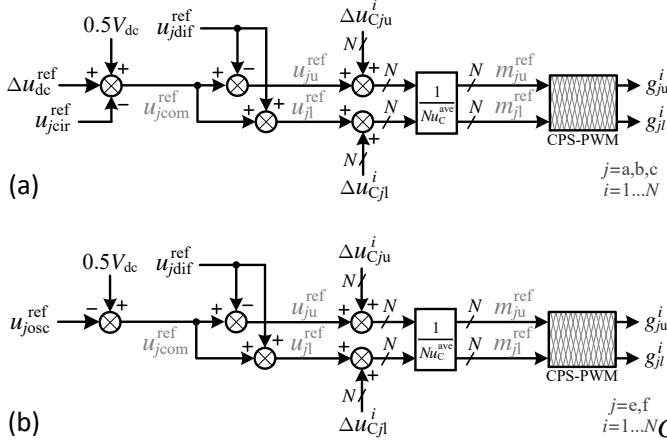


Fig. 16: MMC control reference calculation and modulation

### E. MMC modulation

Modulation indices for each phase can be calculated from the voltage control references:

$$m_{ju} = \frac{u_{jcom}^{\text{ref}} - u_{jdif}^{\text{ref}}}{Nu_{Cj}^{\text{ave}}}, \quad m_{jl} = \frac{u_{jcom}^{\text{ref}} + u_{jdif}^{\text{ref}}}{Nu_{Cj}^{\text{ave}}}. \quad (32)$$

where  $j = a, b, c, e, f$ , and  $u_{jdif}^{\text{ref}}$  is the corresponding value in Fig. 9. In the grid side converter,  $u_{jcom}^{\text{ref}}$  is composed of the feedforward value  $0.5V_{dc}$ , dc voltage stabilising term  $\Delta u_{dc}^{\text{ref}}$  and circulating current control term  $u_{jcir}^{\text{ref}}$ . While in the traction side converter,  $u_{jcom}^{\text{ref}}$  is composed of the feedforward value  $0.5V_{dc}$ , and oscillation suppression control term  $u_{josc}^{\text{ref}}$ . Finally the capacitor voltage balancing terms  $\Delta u_{Cju}^i$  and  $\Delta u_{Cjl}^i$  are added in each submodule. Fig. 16a and Fig. 16b illustrate the control reference calculation and the modulation diagram for grid side MMC and traction side MMC respectively.

## V. SIMULATIONS

The control parameters for the MMC back to back converter are listed in Table III. The measurements in the control system are converted into per-unit system using grid side MMC's power rating as the base value. Three sets of simulation tasks are designed to validate the proposed control scheme. The

TABLE III: Simulation and control parameters setting

MMC control parameters		
Grid side current controller	$[k_p^{idq}, k_i^{idq}]$	[1.5,30]
Traction side voltage controller	$[k_p^{uo}, k_i^{uo}]$	[1.09,84.6]
Double frequency oscillation controller	$[k_p^{uosc}, k_r^{uosc}]$	[1.92,170]
Capacitor average voltage controller	$[k_p^{uc}, k_i^{uc}]$	[1.2,20]
DC voltage stabilisation controller	$[k_p^{udc}, k_i^{udc}, k_d^{udc}]$	[4.40,0.004]
Simulation model time step	$T_s$	5 ms
Controller sampling time	$T_{sc}$	0.1 ms

effectiveness of voltage stabilisation control and voltage oscillation suppression are examined in both steady and transient states. In the conventional MMC rectifier control the dc link voltage is maintained by controlling the submodule capacitors' average voltage which is equivalent to setting  $\Delta u_{dc}^{\text{ref}} = 0$  in the proposed scheme. So in this section, we use  $\Delta u_{dc}^{\text{ref}} = 0$  to represent the conventional control method.

### A. Train load profile and wind power profile

Case A is used to analyse the steady state performance of power delivery on each terminal and the dc voltage quality. Case B<sub>1,2</sub> consider one side step change and test the negative consequences on the other side. Case C<sub>1-4</sub> investigate several worst scenarios that both sides are subject to rated power magnitude step change simultaneously, imposing the severest control challenges on MMC<sub>G</sub>. These simulation tasks are summarised as follow:

Case A  $P_W$  is set to 10 MW;  $P_L$  is set to 0, 5 MW, 10 MW, 20 MW respectively

Case B<sub>1</sub>  $P_W$  is set to 10 MW;  $P_L$  changes from 10 MW to 20 MW then returns to 10 MW

Case B<sub>2</sub>  $P_W$  changes from 0 MW to 10 MW then to 0 MW;  $P_L$  is set to 10 MW

Case C<sub>1</sub>  $P_W$  changes from 10 MW to 0 MW;  $P_L$  changes from 0 MW to 20 MW at the same time

Case C<sub>2</sub>  $P_W$  changes from 0 to 10 MW;  $P_L$  changes from 20 to 0 MW at the same time

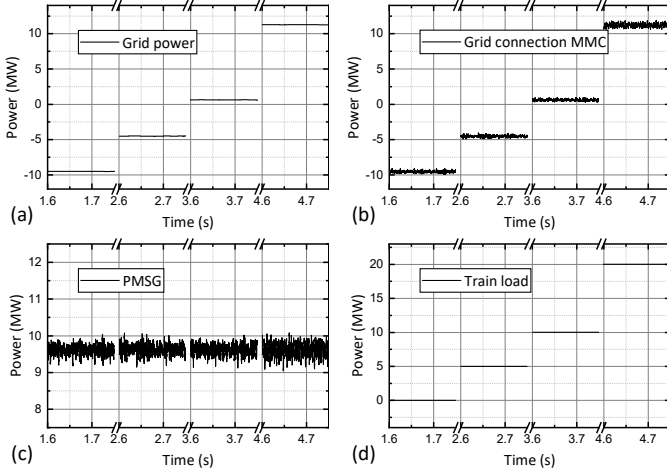
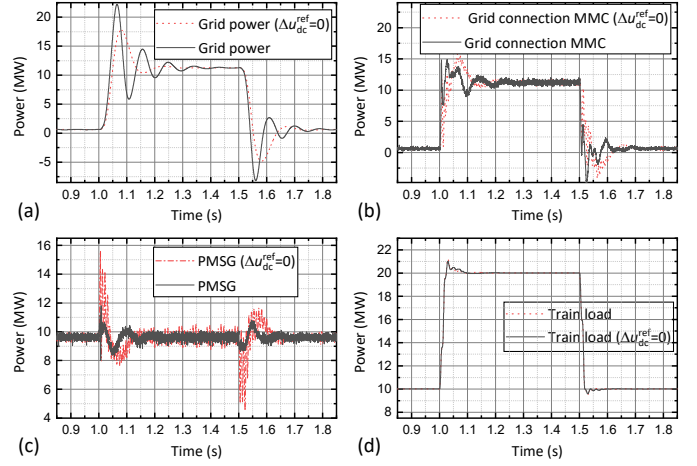
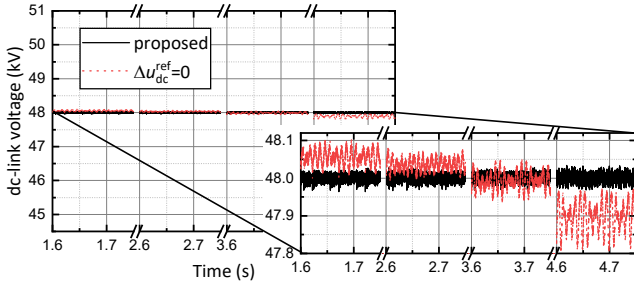
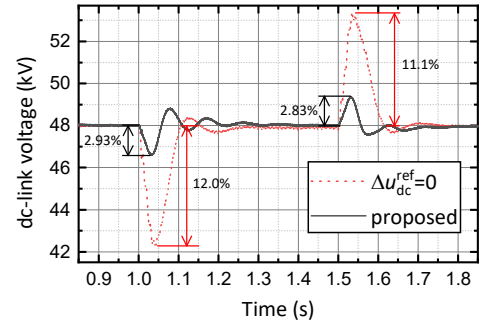
Case C<sub>3</sub>  $P_W$  changes from 0 MW to 10 MW;  $P_L$  changes from 10 MW to -10 MW at the same time

Case C<sub>4</sub>  $P_W$  changes from 10 MW to 0 MW;  $P_L$  changes from -10 MW to +10 MW at the same time

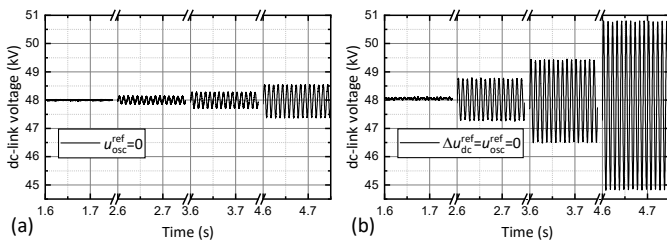
### B. Steady state performance analysis

The power flows across four coupling nodes are measured: three phase ac grid power  $p_{\text{grid}}$ , grid connection MMC dc side power  $p_{\text{mmc}}$ , PMSG converter dc side power  $p_{\text{pmsg}}$  and power consumed by traction load  $p_{\text{train}}$ . These four power flow data are plotted in Fig. 17. In steady states, both ac side power  $p_{\text{grid}}$  and  $p_{\text{train}}$  have very stable values. However  $p_{\text{pmsg}}$  has noisy instantaneous power with ripples at the level of 3.91%–5.38%. As the load power increases, both generation power and MMC power present larger power fluctuations. Because in higher power operation, the MMC has heavier burden to suppress circulating current and maintain dc voltage, and also has larger voltage oscillations in each module.

Figure 18 compares the dc link voltage profiles using the proposed method and the conventional method by setting  $\Delta u_{dc}^{\text{ref}} = 0$  (Fig. 16). Considering the simulation time during 4.6 s to 4.7 s in the largest traction load condition, the proposed method shows less fluctuations (0.068%) than the conventional approach (0.176%). Moreover, when ignoring the dc voltage stabilisation control action, there exists steady state error due to branch inductor voltage drop. The steady state error is reduced from 0.216% to 0.0037% with the proposed control method.

Fig. 17: Steady state power flow (*Case A*)Fig. 20: Instantaneous power flow in *Case B<sub>1</sub>* simulationFig. 18: Steady state dc link voltage comparison 1 (*Case A*)Fig. 21: DC link voltage comparison (*Case B<sub>1</sub>*)

The effects of the proposed control on dc link voltage oscillation suppression is shown in Fig. 19 where the Fig. 19a shows the result of ignoring the oscillation control term  $u_{osc}^{ref}$  and Fig. 19b shows the profile without both proposed control terms. It is evident that Fig. 19b has the greatest voltage ripple caused by single phase traction load. During 4.6 s to 4.7 s, there is large magnitude of steady low frequency oscillation component which contributes to 6.26% voltage ripple. With the help of voltage stabilisation control, the ripple is reduced to 1.23% even we do not control the oscillating current in the traction side MMC. Nevertheless, none of these two cases is acceptable because the existence of 100 Hz oscillation voltage on the dc link is detrimental to stable energy exchange through dc interface. This confirms the necessity of adding the two proposed control loops shown in Fig. 12 and Fig. 13.

Fig. 19: Steady state dc link voltage comparison 2 (*Case A*)

### C. Transient performance analysis

1) *Case B*: *Case B<sub>1</sub>* examines the traction side influence on the PMSG power delivery due to the load change which is first stepped up and then stepped down at 1.0 s and 1.5 s respectively. Improvement brought by the proposed dc voltage controller is plotted in Fig. 20. In both control approaches, these instantaneous power plots all have short time oscillation after load change. Both  $p_{pmsg}$  and  $p_{mmc}$  experienced less fluctuations and less settling time under the extra voltage stabilisation control. The renewable generation will be less affected by the traction load change. The price paid is a greater power overshoot on the grid side.

The greater power oscillations in the wind generation side is caused by deviations in the dc link voltage. As shown in Fig. 21, if  $\Delta u_{dc}^{ref}$  is ignored, the voltage deviation can be as big as 12% in this case study. This problem is greatly alleviated using the proposed control method that only 2.93% voltage dip remains, and the similar results were also observed at 1.5 s. The deviation reduction is above 75%.

*Case B<sub>2</sub>* tests the influence of wind generation fluctuation on the traction side. Similar to the previous results, the proposed control approach reduces power oscillation in all converters except the grid power as shown in Fig. 22. The proposed control again limits the voltage variation within 2.1% of the nominal value which is more than 76% reduction than the conventional approach. It can be seen that, although power change is equal to 10 MW in both case *B<sub>1</sub>* and *B<sub>2</sub>*, the negative

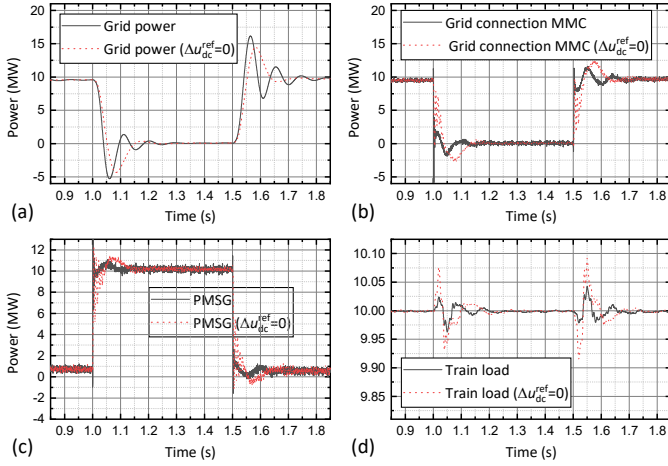


Fig. 22: Instantaneous power flow in *Case B<sub>2</sub>* simulation

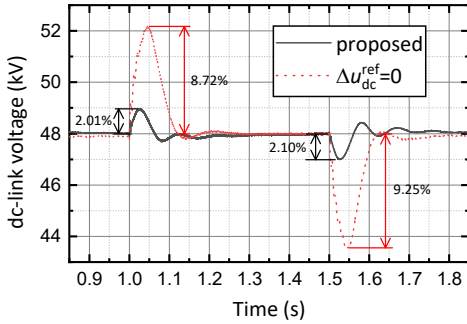


Fig. 23: DC link voltage comparison (*Case B<sub>2</sub>*)

effect brought by wind generation unit is less than traction change, because the generator is a balanced three phase source.

2) *Case C*: The last four scenarios are deliberately designed to test the limit of the system capacity. In these worst cases, although adding  $\Delta u_{dc}^{ref}$  improves dc voltage stability for more than 50%, the largest voltage deviation is still above 14.2%. Fortunately, these situations however rarely occur in real applications, and we can improve the system capacity by increasing the size of capacitor or the converter current rating to withstand these cases if necessary.

3) *Modulation*: Figure 25 shows the voltage control references for upper branch of phase *a* in *Case B<sub>1</sub>*. The voltage reference signals for dc voltage stabilisation, circulating current suppression and ac voltage control are plotted. As explained in Section IV-A, the differential mode modulation signal varies within  $[-0.5, 0.5]$ . And with the voltage stabilisation control, more submodules are switched on to support dc link. As indicated by  $\Delta u_{dc}^{ref}$  line, at 1.18 s, about 9% more modules are inserted in each branch.

The reference  $u_{cir}^{ref}$  also controls the number of inserted modules but the signals for each phase are symmetric. However the  $\Delta u_{dc}^{ref}$  term allows all three phase to shift uniformly to reject voltage fluctuations.

By synthesising all control references based on the method shown in Fig. 16, the final modulation signal is shown in Fig. 26. The result in Fig. 26b is consistent with previous

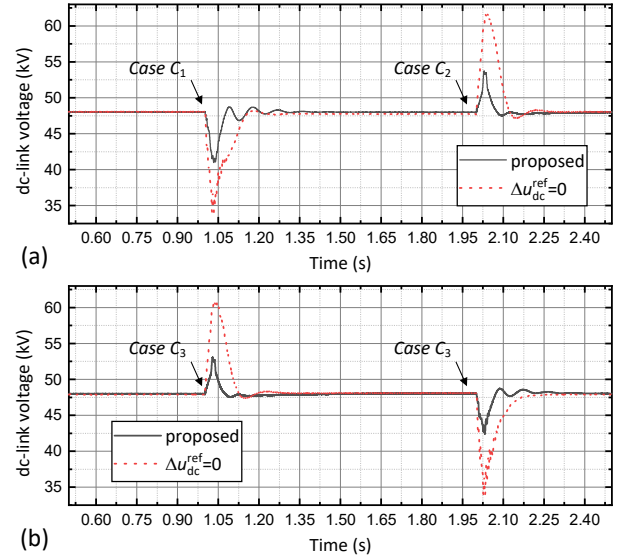


Fig. 24: DC link voltage (*Case C<sub>1-4</sub>*)

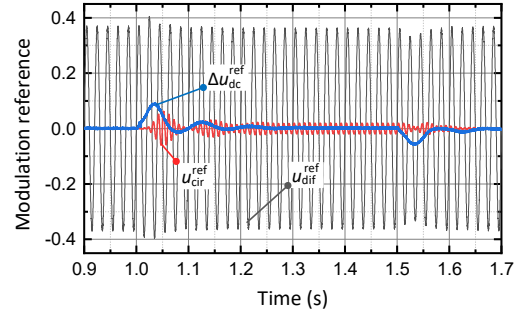


Fig. 25: Voltage references for upper branch of phase A (*Case B<sub>1</sub>*)

analysis that the composite modulation has extra degree of freedom brought by the proposed method. This extra degree of freedom improves the transient response and steady state performance of dc voltage control.

## VI. CONCLUSION

This paper has investigated a feasible connection topology for integrating renewable energy into railway feeder station. A full converter station is realised by the MMC back to back conversion system, the renewable generation is connected to

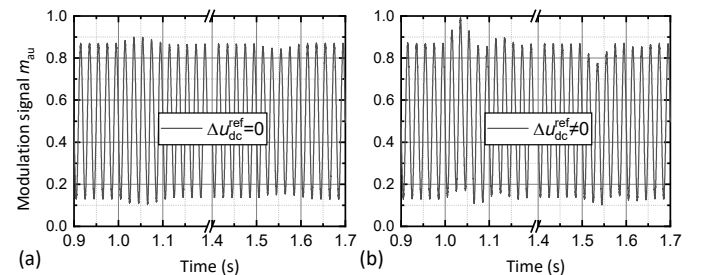


Fig. 26: Comparison of the composite modulation references of phase A upper branch  $m_{au}^{ref}$  (*Case B<sub>1</sub>*)

the dc link inside the MMC. Wind generator is used to supply the traction load or supply to the grid. Other types of RESs can also be integrated in the same way.

The intermittent nature of renewable energy and fast changing characteristic of traction load challenge the stable power delivery. Single phase traction load further aggravates the situation by introducing low frequency oscillating power on the dc link. A systematic approach has been proposed to eliminate the oscillation power issue and reduce voltage deviations in transient response. By controlling common mode reference signal from the current perspective, the traction power supply converter can exchange power through dc link without oscillation. Further by adding extra dc voltage stabilisation control loop, dc voltage is strictly controlled to the rated value in steady state and more than 75% deviation on 10 MW step change can be reduced.

Modelling and design considerations for the MMC back to back conversion system are explained under this control approach. The advantage of the proposed scheme is that the internal control freedom of MMC system is further utilised to actively solve these issues without resorting to large passive devices.

In conclusion, the proposed system is shown to provide a stable dc link interface for renewable integration in the railway traction supply system, and has the potential to save the investment cost for grid connection converter in RES. Energy storage system can also be interfaced with the dc bus to mitigate the intermittent renewable energy while still benefits from the stable dc voltage performance.

#### REFERENCES

- [1] José Antonio Aguado, Antonio José Sánchez Racero, and Sebastián de la Torre. "Optimal operation of electric railways with renewable energy and electric storage systems". In: *IEEE Transactions on Smart Grid* 9.2 (2016), pp. 993–1001.
- [2] Trevor Bagnall, Francisco Siliezar, et al. "Power electronics based traction power supply for 50Hz railways". In: *CORE 2014: Rail Transport For A Vital Economy* (2014), p. 413.
- [3] Taylor Egan et al. "Design and control of resilient interconnected microgrid for sustained railway". In: *2017 IEEE International Conference on Smart Energy Grid Engineering (SEGE)*. IEEE. 2017, pp. 131–136.
- [4] Eduardo Pilo de la Fuente, Sudip K Mazumder, and Ignacio González Franco. "Railway Electrical Smart Grids: An introduction to next-generation railway power systems and their operation." In: *IEEE Electrification Magazine* 2.3 (2014), pp. 49–55.
- [5] Hitoshi Hayashiya et al. "Comparative study of investment and efficiency to reduce energy consumption in traction power supply: A present situation of regenerative energy utilization by energy storage system". In: *2014 16th International Power Electronics and Motion Control Conference and Exposition*. IEEE. 2014, pp. 685–690.
- [6] Hitoshi Hayashiya et al. "Possibility of energy saving by introducing energy conversion and energy storage technologies in traction power supply system". In: *2013 15th European Conference on Power Electronics and Applications (EPE)*. IEEE. 2013, pp. 1–8.
- [7] Hitoshi Hayashiya et al. "Potentials, peculiarities and prospects of solar power generation on the railway premises". In: *2012 International Conference on Renewable Energy Research and Applications (ICRERA)*. IEEE. 2012, pp. 1–6.
- [8] Jin Huang et al. "Harmonic current elimination for single-phase rectifiers based on PR controller with notch filter". In: *2012 15th International Conference on Electrical Machines and Systems (ICEMS)*. IEEE. 2012, pp. 1–5.
- [9] Y. Jing et al. "Enhanced AC voltage and frequency control of offshore MMC station for wind farm connection". In: *IET Renewable Power Generation* 12.15 (2018), pp. 1771–1777. ISSN: 1752-1424.
- [10] Ivan Krastev et al. "Future of electric railways: advanced electrification systems with static converters for ac railways". In: *IEEE Electrification Magazine* 4.3 (2016), pp. 6–14.
- [11] Y. LI, Y. Li, and Q. Wang. "Robust Predictive Current Control with Parallel Compensation Terms against Multi-parameter Mismatches for PMSMs". In: *IEEE Transactions on Energy Conversion* (2020), pp. 1–1.
- [12] Yuanli Liu et al. "Energy Management of Connected Co-Phase Traction Power System Considering HESS and PV". In: *2019 14th IEEE Conference on Industrial Electronics and Applications (ICIEA)*. IEEE. 2019, pp. 1408–1412.
- [13] Fujun Ma et al. "Multi-Port Railway Power Conditioner and Its Management Control Strategy with Renewable Energy Access". In: *IEEE Journal of Emerging and Selected Topics in Power Electronics* (2019).
- [14] B. Mitra, B. Chowdhury, and M. Manjrekar. "HVDC transmission for access to off-shore renewable energy: a review of technology and fault detection techniques". In: *IET Renewable Power Generation* 12.13 (2018), pp. 1563–1571. ISSN: 1752-1424. DOI: 10.1049/iet-rpg.2018.5274.
- [15] Hrvoje Novak, Vinko Lešić, and Mario Vašak. "Hierarchical Model Predictive Control for Coordinated Electric Railway Traction System Energy Management". In: *IEEE Transactions on Intelligent Transportation Systems* 20.7 (2018), pp. 2715–2727.
- [16] İbrahim Şengör et al. "Energy management of a smart railway station considering regenerative braking and stochastic behaviour of ESS and PV generation". In: *IEEE Transactions on Sustainable Energy* 9.3 (2017), pp. 1041–1050.
- [17] Daniel Serrano-Jiménez et al. "Electrical railway power supply systems: Current situation and future trends". In: *International Journal of Electrical Power & Energy Systems* 92 (2017), pp. 181–192.

- [18] Kamran Sharifabadi et al. *Design, control, and application of modular multilevel converters for HVDC transmission systems*. John Wiley & Sons, 2016.
- [19] Yingyun Sun et al. “Battery-based energy storage transportation for enhancing power system economics and security”. In: *IEEE Transactions on Smart Grid* 6.5 (2015), pp. 2395–2402.
- [20] Abel A Taffese et al. “Power oscillation damping with virtual capacitance support from modular multilevel converters”. In: *IET Renewable Power Generation* 14.5 (2020), pp. 897–905.
- [21] Montie Alves Vitorino et al. “Low-frequency power decoupling in single-phase applications: A comprehensive overview”. In: *IEEE Transactions on Power Electronics* 32.4 (2016), pp. 2892–2912.
- [22] Yizhen Wang et al. “DC voltage deviation-dependent voltage droop control method for VSC-MTDC systems under large disturbances”. In: *IET Renewable Power Generation* 14.5 (2019), pp. 891–896.
- [23] Zheng Xu, Huangqing Xiao, and Zheren Zhang. “Selection methods of main circuit parameters for modular multilevel converters”. In: *IET Renewable Power Generation* 10.6 (2016), pp. 788–797.
- [24] L. Yu, R. Li, and L. Xu. “Hierarchical control of offshore wind farm connected by parallel diode-rectifier-based HVDC and HVAC links”. In: *IET Renewable Power Generation* 13.9 (2019), pp. 1493–1502. ISSN: 1752-1424. DOI: 10.1049/iet-rpg.2019.0033.
- [25] Xueyang Zeng et al. “Coordinated control of MMC-HVDC system with offshore wind farm for providing emulated inertia support”. In: *IET Renewable Power Generation* 14.5 (2019), pp. 673–683.
- [26] Xiaojuan Zhu et al. “Stability analysis of pv plant-tied MVdc railway electrification system”. In: *IEEE Transactions on Transportation Electrification* 5.1 (2019), pp. 311–323.